

# A Simple Baseline for Supervised Surround-view Depth Estimation

Xianda Guo <sup>1</sup>Wenjie Yuan <sup>2</sup>Yunpeng Zhang <sup>1</sup>Tian Yang <sup>1</sup>Chenming Zhang <sup>3</sup>Zheng Zhu <sup>1,†</sup>

## Abstract

*Depth estimation has been widely studied and serves as the fundamental step of 3D perception for autonomous driving. Though significant progress has been made for monocular depth estimation in the past decades, these attempts are mainly conducted on the KITTI benchmark with only front-view cameras, which ignores the correlations across surround-view cameras. In this paper, we propose **S3Depth**, a Simple Baseline for Supervised Surround-view Depth Estimation, to jointly predict the depth maps across multiple surrounding cameras. Specifically, we employ a global-to-local feature extraction module which combines CNN with transformer layers for enriched representations. Further, the **Adjacent-view Attention** mechanism is proposed to enable the intra-view and inter-view feature propagation. The former is achieved by the self-attention module within each view, while the latter is realized by the adjacent attention module, which computes the attention across multi-cameras to exchange the multi-scale representations across surround-view feature maps. Extensive experiments show that our method achieves superior performance over existing state-of-the-art methods on both DDAD and nuScenes datasets.*

## 1. Introduction

With the rapid development of autonomous driving technology in recent years, depth estimation has received increasingly more attention. As a bridge connecting the 2D images and the 3D environments, depth estimation aims to recover the dense 3D representations from 2D images. Monocular depth estimation [11, 12, 49, 39, 30, 63, 24, 69, 13, 73] aims to get the depth map of a single image, which either uses LiDAR points as the target depth or learns from monocular videos in a self-supervised manner. Although significant progress has been made for monocular

<sup>1</sup> PhiGent Robotics, xianda.guo@163.com, {yunpeng.zhang, tian.yang}@phigent.ai, zhengzhu@ieee.org

<sup>2</sup> School of Information Science and Technology, Dalian Maritime University, yuanwenjie@dlmu.edu.cn

<sup>3</sup> School of Computer and Information technology, Beijing Jiaotong University, chmzhang@bjtu.edu.cn

† Corresponding Author

depth estimation in the past decade, existing methods are mainly performed on only a few driving scenes, mostly KITTI datasets [14]. Stereo matching [42, 44, 37, 20, 64, 53, 55, 27, 7, 28, 72, 66, 8, 35] attempts to predict the disparity between the left and right camera images, where a large overlap between the stereo images are essentially assumed. Though these methods achieve impressive performance for depth estimation, their receptive fields are limited to a small fraction of the entire 3D environment (usually less than 180°).

Although recently released datasets contain consistent multi-camera data that capture the full 360° point cloud [17, 5], existing methods still handle the problems as monocular [1, 11, 12, 49, 39, 30, 63, 24, 69, 13, 73] and ignore the multi-view interaction. Multi-View Stereo [68, 65, 60, 65, 26] is an effective method to predict a depth map by a series of calibrated images surrounding an object, but it needs large overlapping areas between cameras.

FSM [19] firstly extends self-supervised learning from monocular and stereo to the general multi-camera setting and introduces spatial-temporal contexts and pose consistency constraints, which boost performance in multi-camera settings. Following FSM [19], SurroundDepth [61] proposes to jointly process all surrounding views by the module of cross-view attention to get high-quality depth maps. In addition, SurroundDepth [61] is able to get the depths with real-world scales by the scale-aware SfM pretraining. However, the performance of these methods is insufficient for practical applications.

Multi-view 3D object detection in Bird's-Eye-View (BEV) has received great attention in recent years, because it has a much lower computational cost for autonomous driving than LiDAR-based solutions. Estimating accurate depth is essential for multi-view 3D object detection. However, it remains challenging to predict depth in surrounding images without overlapping areas. BEVDepth [34] provides a quantitative and qualitative analysis of depth estimation within 3D detectors, and boosts the performance of 3D detectors by using ground-truth depth. This reveals that accurate depth is helpful for multi-view 3D object detection. Based on BEVDepth [34] and inspired by the success of the MVS and monocular depth estimation methods [68, 59, 62, 18, 2], STS [57] proposes the temporal stereo technique called Surround-view Temporal Stereo (STS), which lever-

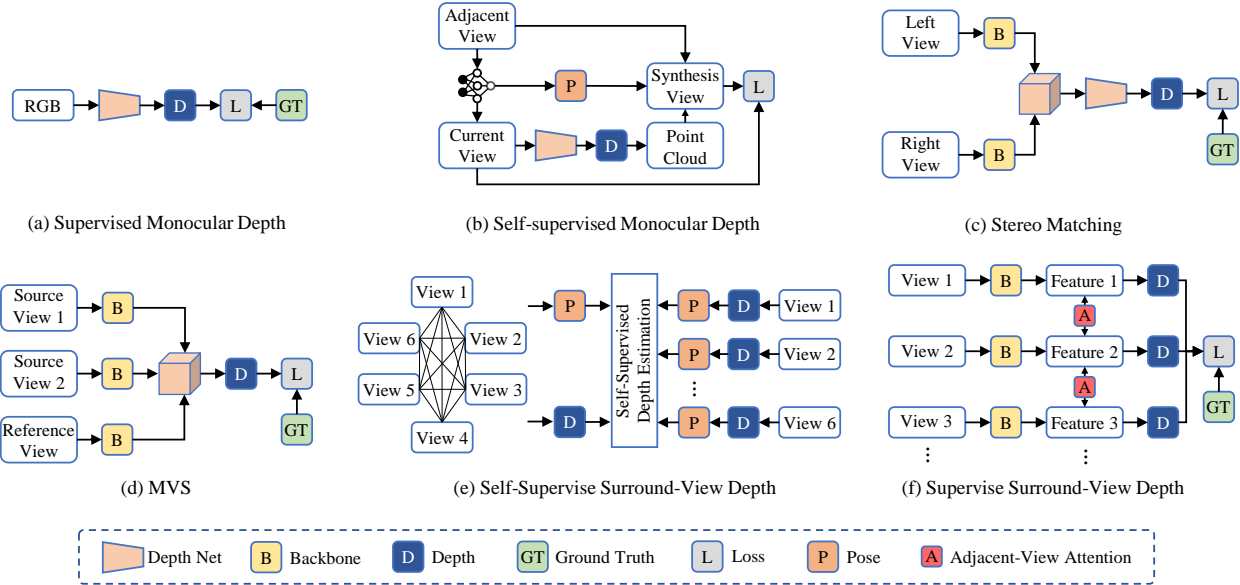


Figure 1. Paradigm comparison of Supervised Monocular Depth, Self-supervised Monocular Depth, Stereo Matching, Multi-View Stereo (MVS), Self-supervised Surround-View Depth and Supervised Surround-View Depth.

ages the geometric correspondence across frames over time. Different from BEVDepth [34] which predicts depth from a single image, BEVStereo [33] further predicts both the monocular and stereo depths to get better BEV representations for 3D object detection. Although these methods have explored the effect of depth estimation on BEV 3D object detection, there is no baseline for supervised surround-view depth estimation.

In this paper, we propose a Simple Baseline for Supervised Surround-view Depth estimation, called **S3Depth**. Specifically, we first employ a shared encoder which can extract global-to-local features by combining CNN with transformer layers. To learn adjacent-view interactions in surrounding views, we adopt the alternating attention mechanism: self-attention computes attention in the same view, while adjacent attention computes attention between adjacent views. Finally, different from monocular depth estimation, a Depth Head is used to predict all surround-view depth maps at the same time. We conduct extensive experiments on the challenging datasets DDAD [17] and nuScenes [5] for multi-camera depth estimation. Experimental results show that the adjacent-view feature interaction boosts the performance of depth estimation.

In summary, the main contributions are as follows:

- For the first time, we propose a simple baseline for supervised surround-view depth Estimation, to jointly predict depth maps in a wide-baseline 360° multi-camera setting.
- We use the joint convolutional attention and trans-

former block for surround-view depth estimation to model local and global contexts.

- We propose **Adjacent-view Attention** mechanism which can be used to enable the intra-view and inter-view feature propagation in this novel setting.
- Our S3Depth yields substantial improvements to depth estimation when compared to state-of-the-art methods on two publicly available multi-camera datasets: *DDAD* [17] and *nuScenes* [5].

## 2. Related Work

**Monocular Depth Estimation.** Monocular depth estimation has been studied in computer vision for a long time and plays a crucial role in 3D reconstruction, autonomous driving cars and robot navigation. Supervised approaches take a single image and use datasets collected by laser scanners [14] or other range sensors [43] as target depth labels in training, as shown in Figure 1(a). Although learning-based depth estimation methods [11, 12, 49, 39, 30, 63, 24, 69, 13, 36, 1, 46, 52, 38, 71] achieve impressive results when compared with traditional machine learning baselines [50, 77, 40], these methods need additional sensors which are used to collect “ground-truth” data. Besides, these methods are designed for the KITTI datasets [14] whose “ground-truth” depth maps are dense. Moreover, the “ground-truth” data may be sparsity and not be very reliable due to high noise during data collection in practical applications. Thus, self-supervised methods [76, 58, 7, 70, 15, 3, 75, 48, 74] explore the routes of

jointly learning monocular depth and ego-motion from unlabelled sequential data, as shown in [Figure 1\(b\)](#). Zhou *et al.* [76] convert the monocular depth estimation into a task of view synthesis, using the photometric loss as the supervisory signal to train networks to separately predict poses and depths. To enhance the quality of predictions, Monodepth2 [15] presents an auto-masking loss and a minimum reprojection loss, which can handle occlusions and moving objects. PackNet-Sfm [17] introduces a new 3D convolution called PackNet, which can run in real-time at high resolution, and a novel loss. Recently, inspired by the success of transformer [10, 41, 32, 47, 67, 18], MonoVit [73] further improved depth estimation accuracy by combining plain convolutions with transformer blocks. However, these approaches are designed for monocular depth estimation (typically less than 180°), consistent surround-view depth estimation would extend these approaches to the full 360° space.

**Stereo Matching.** Stereo matching attempts to predict disparity between the left and right camera image, which can be used to estimate depth, as shown in [Figure 1\(c\)](#). In general, the stereo depth estimation task treats the 2D matching problem as a 1D disparity search. Traditional methods [22, 23] utilize hand-crafted features to compute matching cost, which tends to fail on those textureless and repetitive regions in the images. In recent years, with the support of large synthetic datasets [42, 4, 54], the end-to-end network has achieved impressive performance on stereo matching. One line of networks [42, 44, 37, 20, 64, 53, 55] match features by dot-product correlation, which only uses 2D convolutions. Another line of networks [27, 7, 28, 72, 66, 8] build 4D features volume and learn to aggregate the matching cost by 3D convolutions. Besides, Li *et al.* [35] take advantage of the transformer architecture, which has advantages in feature matching and relaxes the limitation of a fixed disparity range, and presents a new end-to-end-trained network called STTR. However, a large overlap between left and right images is needed to train these models. Our proposed method is intended for consistent multi-camera configurations with minimal image overlap.

**Surround-view Depth Estimation.** Based on the way of supervision, surround-view depth estimation methods can be divided into self-supervised and supervised. To our knowledge, FSM [19] firstly extends self-supervised monocular depth estimation to a large-baseline multi-camera setting. Following FSM [19], SurroundDepth [61] recovers the real-world scales by pretraining the depth network with sparse depths obtained from SfM [51] and learn to capture the surround-view interactions by the module of cross-view attention, as shown in [Figure 1\(e\)](#). For the task of supervised multi-view depth estimation, it is an effective method to build cost volume [68, 65, 60, 65, 26], namely, multi-view stereo (MVS). MVS aims to estimate the depth

map by a series of calibrated images surrounding an object, and it is a one-to-many feature matching task, as shown in [Figure 1\(d\)](#). Different from MVS, our model is designed to estimate all depth maps of surrounding multi-view images with small overlapping areas between cameras.

Our multi-camera setting is related to the works [34, 33, 57], where consistent multi-camera depth maps are used to predict 3D bounding boxes. BEVDepth [34] introduces a depth correction module supervised explicitly by LiDAR, which encodes the camera parameters and is helpful for 3D object detection. Inspired by the success of the MVS and monocular depth estimation methods [68, 59, 62, 18, 2], STS [57] proposes the temporal stereo technique called Surround-view Temporal Stereo (STS), which is used to facilitate 3D detection. To get better BEV representations for 3D object detection, BEVStereo [33] enhances depth estimation with dynamic temporal stereo, which is able to handle complex outdoor scenarios. Although those methods [34, 57, 33] have explored the effect of depth estimation on 3D object detection, there has been a lack of a baseline for supervised surround-view depth estimation. Therefore, it is necessary to establish a simple yet effective baseline for supervised surround-view depth estimation in order to evaluate the performance of more advanced methods and facilitate the development of this research field.

### 3. Proposed Method

#### 3.1. Problem Formulation

Given  $N$  views input samples  $I = \{I^1, I^2, \dots, I^N\}$ , the surround-view depth model  $f(\cdot)$  is expected to predict the depth map  $D^{pred} = \{D_1^{pred}, D_2^{pred}, \dots, D_N^{pred}\}$ , where  $I^i \in \mathbb{R}^{H \times W \times 3}$  denotes the surround-view RGB images,  $D_i^{pred} \in \mathbb{R}^{H \times W}$  denotes the predicted depth map and  $H, W$  stand for the height and width of input images, respectively. In S3Depth, the only supervised signal comes from LiDAR. Different from monocular depth estimation, there are crucial overlaps across the surround-view images, which are very useful and can be imported for the model to understand the scene as a whole. Based on that, we introduce a simple baseline S3Depth to predict 360° view depth at the same time. By taking advantage of the adjacent-view information interactions, S3Depth can achieve better performance of every view than view-dependent estimations.

#### 3.2. Overview

[Figure 2](#) shows our proposed S3Depth architecture. Our purpose is to build a powerful baseline for dense depth prediction of surround-view images, so we employ a multi-stage model [32] to get enriched representations. Specifically, the baseline consists of three parts: Feature Extraction, Adjacent-view Attention and Depth Head. (1) Feature extraction is a shared backbone that extracts 2D features

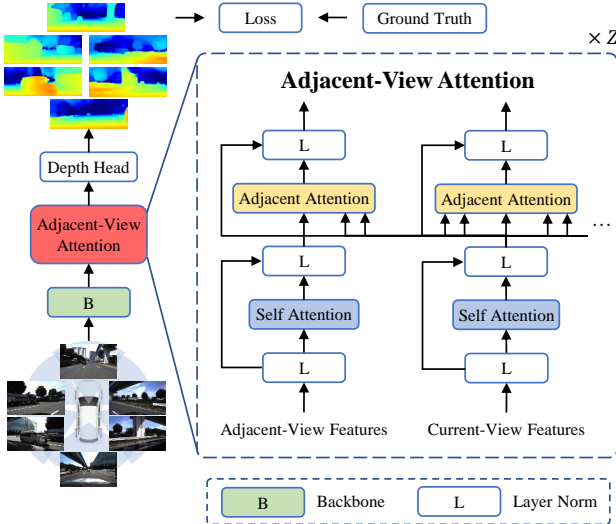


**Figure 2. The architecture of our proposed S3Depth.** Our S3Depth consists of three part: Feature Extraction, Adjacent-view Attention and Depth Head. For feature extraction, both transformer and convolutional layers are adopted to enhance the feature modeling and depth inferring. For Adjacent-view Attention, the alternating self-attention and adjacent-attention are adopted for  $Z$  times to fully exchange the information between current view and adjacent view. Finally, Depth Head predicts the all-view depth map at the same time.

from  $N$  views of input images. (2) The adjacent-View Attention architecture is leveraged to exchange adjacent-view information of features. Specifically, the alternating attention mechanism is adopted: self-attention computes attention to features in the same view, while adjacent-attention computes attention to features in the adjacent views to exchange the adjacent multi-scale representations at every scale. (3) Different from monocular depth estimation, the Depth Head predicts the surround-view depth map at the same time.

### 3.3. Feature Extractor

**Image Encoder.** Recently, the attention mechanism has already proven to be effective in various computer vision tasks, such as image classification [41], object detection [6] and depth estimation [47, 67, 18, 73]. Benefiting from the inductive bias, the transformer allows the model to focus on the important parts of the feature. Although the transformer can model global context perception, it may ignore local relationships. On the contrary, CNN can take advantage of local connectivity. Therefore, we adopt a module that combines CNN with transformer [32] within S3Depth, as shown in Figure 3, which can learn to interact between local and global features for enriched representations in five stages. Specifically, in the first stage, a Conv-stem block is adopted to extract 2D features  $F_1 \in \mathbb{R}^{N \times C_F \times \frac{H}{2} \times \frac{W}{2}}$ , where  $H$  and  $W$  indicate the height and

width of images,  $N$  represents views of input images and  $C_F$  stands for the feature channel number. For the next four stages  $i \in \{2, 3, 4, 5\}$ , the joint convolution attention and transformer blocks are used to extract a features pyramid  $\{F_2 \in \mathbb{R}^{N \times C_F \times \frac{H}{2} \times \frac{W}{2}}, F_3 \in \mathbb{R}^{N \times C_F \times \frac{H}{4} \times \frac{W}{4}}, F_4 \in \mathbb{R}^{N \times C_F \times \frac{H}{8} \times \frac{W}{8}}, F_5 \in \mathbb{R}^{N \times C_F \times \frac{H}{16} \times \frac{W}{16}}\}$ , which can represent multi-scale features.

**Depth Decoder.** In the depth decoder, we fuse the multi-scale features of the same view and the features of cross-view images, and gradually increase the spatial resolution. Then, the features are aggregated at  $\frac{1}{2}, \frac{1}{4}, \frac{1}{8}, \frac{1}{16}$  resolutions respectively. Moreover, the output maps at  $\frac{1}{2}, \frac{1}{4}, \frac{1}{8}, \frac{1}{16}$  resolutions are upsampled to the input resolution and then compute the loss function. Finally, a skip connection is utilized to connect input and output features for reducing the information loss of downsampled feature maps.

### 3.4. Adjacent-view Attention

The detailed structure of the adjacent-view attention architecture is provided in Figure 2. Different from SurroundDepth [61], we adopt the alternating self-attention and adjacent-attention. Self-attention extracts features within the current view and adjacent-attention are used to exchange representations across adjacent view features. Let  $F_{ij} \in \mathbb{R}^{N \times C_F \frac{H}{n} \times \frac{W}{n}}, i = 1, 2, 3, 4, 5, j = 1, 2, 3, 4, 5, n$  be the feature maps obtained from the  $j$ -th view of the  $i$ -th stage, where  $H$  and  $W$  indicates the height and width of images,  $N$  represents views of input images,  $C_F$  stands for the feature channel number. For every stage, multi-head attention is used to increase the expressiveness of the features. The attention mechanism uses the dot product similarity to calculate the attention between the *query* vectors and the *key* vectors, and then weigh the *value* vectors. For self-attention, the  $\mathcal{Q}, \mathcal{K}, \mathcal{V}$  are computed from the same view using feature descriptors  $F_{ij}$  as input, where  $W_{\mathcal{Q}}, W_{\mathcal{K}}, W_{\mathcal{V}} \in \mathbb{R}^{C \times C}, b_{\mathcal{Q}}, b_{\mathcal{K}}, b_{\mathcal{V}} \in \mathbb{R}^C$  and  $C$  represents the embedding dimension respectively:

$$\begin{aligned}
 Q_{i,j} &= W_{\mathcal{Q}}F_{i,j} + b_{\mathcal{Q}} \\
 K_{i,j} &= W_{\mathcal{K}}F_{i,j} + b_{\mathcal{K}} \\
 V_{i,j} &= W_{\mathcal{V}}F_{i,j} + b_{\mathcal{V}} \\
 F_{i,j}^{sf} &= \text{softmax}\left(\frac{Q_{i,j}^T K_{i,j}}{\sqrt{C}}\right)V_{i,j}
 \end{aligned} \tag{1}$$

For adjacent-attention,  $\mathcal{K}, \mathcal{V}$  are computed from the current-view feature, while  $\mathcal{Q}$  is computed from the adjacent-view feature, where  $x$  refers to adjacent views ( $x \in j-1, j+1$ ):

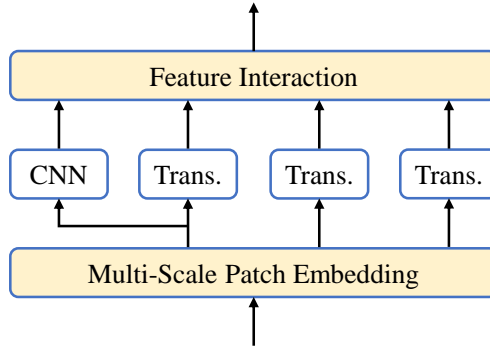


Figure 3. The module combining CNN and Transformer layers.  
Trans stands for Transformer.

$$\begin{aligned}
 Q_{i,x} &= W_Q F_{i,x}^{sf} + b_Q \\
 K_{i,j} &= W_K F_{i,j}^{sf} + b_K \\
 V_{i,j} &= W_V F_{i,j}^{sf} + b_V \\
 F_{i,j}^{adj} &= \text{softmax}\left(\frac{Q_{i,x}^T K_{i,j}}{\sqrt{C}}\right) V_{i,j}
 \end{aligned} \tag{2}$$

To make information fully interactive between the current view and adjacent views, the alternating self-attention and adjacent-attention are used for  $Z$  times.

### 3.5. Depth Head.

To achieve a comprehensive understanding and powerful representation, features at the same location at different scales are used together to predict the final depth. By taking advantages of the adjacent-view attention, features can interact with adjacent views to compensate for erroneous estimations. Let  $F^{out}$  denote the features from the Depth decoder and adjacent-attention, the final output can be represented as follows:

$$F^{final} = \sigma(F^{out}) D_{max} \tag{3}$$

where  $\sigma$  stands for the *sigmoid* activation function and  $D_{max}$  denotes the max distance.

### 3.6. Loss Function

We directly use point cloud data as supervision for the depth estimation. Specifically, the point cloud is projected onto the image plane.  $L_1$  loss is adopted to calculate the distance with the ground-truth depth on the valid pixels as follows:

$$L_{depth} = \frac{1}{N_{valid}} \sum_i (D^{gt} > 0) \left| D_i^{pred} - D_i^{gt} \right| \tag{4}$$

where  $N_{valid}$  stands for the number of valid pixels,  $(D^{gt} > 0)$  indicates whether a pixel has the corresponding point

cloud for ground-truth depth,  $D^{pred}$  denotes the predicted depth, and  $D^{gt}$  represents the ground-truth depth.

Inspired by recent self-supervised depth estimation [16] methods, an  $L_1$  penalty on the depth map is used to encourage local smoothness.

$$L_{smooth} = \sum_x |\partial_x d'_x| e^{-\|\partial_x I_x\|} + |\partial_y d'_x| e^{-\|\partial_y I_x\|} \tag{5}$$

Finally, we combine  $L_{depth}$  and  $L_{smooth}$  to supervise the network:

$$L = L_{depth} + \lambda L_{smooth} \tag{6}$$

## 4. Experiments

### 4.1. Datasets

We conduct experiments on both the nuScenes datasets [5] and Dense Depth for Automated Driving (DDAD) [17].

**NuScenes** [5]. The nuScenes benchmark is an up-to-date dataset for 3D object detection, as well as semantic segmentation, which is captured in both Boston and Singapore by using a capture system with six cameras, one LiDAR and five radars. It collects 1000 scenes which are divided into 700/150/150 scenes for training/validation/testing. The ground truth depths are generated by processing LiDAR point cloud. However, conducting supervised depth on the nuScenes dataset is difficult because of the sparse point cloud and relatively small overlap across cameras. Thus, it has not been applied as the benchmark for supervised surround-view depth evaluation so far. We introduce a simple baseline, which is robust enough to achieve state-of-the-art performance on this dataset by a large margin, compared with previous methods. During the training and evaluation procedure, we consider the max distance  $D_{max}$  as 80m.

**DDAD** [17]. The DDAD dataset is a large-scale dataset for long-range (up to 250m) and dense depth estimation in challenging conditions. The dataset is collected by six cameras and a high-resolution Luminar-H2, which is used to generate dense ground-truth depth maps. There are 12,650 training samples (75,900 images) and 3,950 validation samples (15,800 images) in this dataset. Compared to other related methods, S3Depth can first establish a baseline for surround-view depth estimation. During the training and evaluation procedure, we consider the max distance  $D_{max}$  as 200m.

**Evaluation Metrics.** We assess the results of our method following the evaluation protocol of the depth estimation task [15, 17, 19, 61]. Specifically, we report seven standard metrics (mean Absolute Relative error (Abs Rel), mean Squared Relative error (Sq Rel), Root Mean Squared Error (RMSE), RMSE log,  $\delta < 1.25$ ,  $\delta < 1.25^2$ ,  $\delta < 1.25^3$ ). While evaluating self-supervised depth estimation methods, the scores are averaged per-frame with median-scaling [19, 61].

Method	Resolution	Train	Test	lower is better				higher is better		
				Abs Rel $\downarrow$	Sq Rel $\downarrow$	RMSE $\downarrow$	RMSE log $\downarrow$	$\delta_1 \uparrow$	$\delta_2 \uparrow$	$\delta_3 \uparrow$
Monodepth2* [15]	900 $\times$ 1600	S	MS	0.287	3.349	7.184	0.345	0.641	0.845	0.925
PackNet-SfM* [17]	900 $\times$ 1600	S	MS	0.309	2.891	7.994	0.390	0.547	0.796	0.899
FSM [19]	900 $\times$ 1600	S	MS	0.299	-	-	-	-	-	-
FSM* [19]	900 $\times$ 1600	S	MS	0.334	2.845	7.786	0.406	0.508	0.761	0.894
SurroundDepth* [61]	900 $\times$ 1600	S	MS	0.245	3.067	6.835	0.321	0.719	0.878	0.935
BTS $^\dagger$ [31]	900 $\times$ 1600	D	-	0.253	1.919	6.425	0.348	0.607	0.826	0.914
PixelFormer $^\dagger$ [1]	900 $\times$ 1600	D	-	0.099	0.553	3.171	0.165	0.904	0.959	0.979
SurroundDepth $^\dagger$ [61]	900 $\times$ 1600	D	-	0.158	1.189	5.028	0.239	0.813	0.930	0.965
Ours	900 $\times$ 1600	D	-	<b>0.067</b>	<b>0.673</b>	<b>2.457</b>	<b>0.144</b>	<b>0.951</b>	<b>0.970</b>	<b>0.981</b>

Table 1. Quantitative depth estimation results on the nuScenes [5] dataset. The symbol \* indicates the implementation of SurroundDepth [61]. Resolution refers to the resolution of evaluation. The symbol  $^\dagger$  indicates our implementations. S denotes self-supervised, D denotes depth supervision with Lidar and MS indicates that the scores are averaged per-frame with median-scaling [19, 61] at test time.

Method	Resolution	Train	Test	lower is better				higher is better		
				Abs Rel $\downarrow$	Sq Rel $\downarrow$	RMSE $\downarrow$	RMSE log $\downarrow$	$\delta_1 \uparrow$	$\delta_2 \uparrow$	$\delta_3 \uparrow$
Monodepth2* [15]	1216 $\times$ 1936	S	MS	0.362	14.404	14.178	0.412	0.683	0.859	0.922
PackNet-SfM* [17]	1216 $\times$ 1936	S	MS	0.301	5.339	14.115	0.395	0.624	0.828	0.908
Monodepth2 -M*	1216 $\times$ 1936	S	MS	0.217	3.641	12.962	0.323	0.699	0.877	0.939
PackNet-SfM -M*	1216 $\times$ 1936	S	MS	0.234	3.802	13.253	0.331	0.672	0.860	0.931
FSM [19]	1216 $\times$ 1936	S	MS	0.202	-	-	-	-	-	-
FSM* [19]	1216 $\times$ 1936	S	MS	0.229	4.589	13.520	0.327	0.677	0.867	0.936
SurroundDepth* [61]	1216 $\times$ 1936	S	MS	0.200	3.392	12.270	0.301	0.740	0.894	0.947
BTS $^\dagger$ [31]	1216 $\times$ 1936	D	-	0.290	4.378	14.563	0.410	0.497	0.766	0.904
PixelFormer $^\dagger$ [1]	1216 $\times$ 1936	D	-	0.177	2.525	11.048	0.271	0.747	0.923	0.957
SurroundDepth $^\dagger$ [61]	1216 $\times$ 1936	D	-	0.175	2.694	11.607	0.283	0.757	0.905	0.953
Ours	1216 $\times$ 1936	D	-	<b>0.160</b>	<b>2.527</b>	<b>10.803</b>	<b>0.263</b>	<b>0.799</b>	<b>0.922</b>	<b>0.960</b>

Table 2. Comparisons for surround-view depth estimation on DDAD dataset [17]. Resolution refers to evaluating resolution. -M indicates occlusion masking. \* indicates the implementation of SurroundDepth [61]. The symbol  $^\dagger$  indicates our implementations. S denotes self-supervised, D denotes depth supervision with Lidar and MS indicates that the scores are averaged per-frame with median-scaling [19, 61] at test time.

## 4.2. Implementation Details

**BTS** We use the official implementation of BTS [31]. Densenet161 [25] is used as the backbone. The number of epochs is set to 10 for nuScenes and 20 for DDAD. Silog is employed as the loss function.

**PixelFormer** We use the official implementation of PixelFormer [1]. Swin-Tiny [41] is used as the backbone. The number of epochs is set to 10 for nuScenes and 20 for DDAD. Silog is employed as the loss function.

**SurroundDepth** [61] We use the official implementation of SurroundDepth [61], and only change the supervision from self-supervised to LiDAR supervised. L1 loss is employed for training the model.

**S3Depth** We conduct experiments on both DDAD [17] and nuScenes [5] datasets for depth estimation. S3Depth is implemented with the deep-learning library PyTorch [45]. We employ MPViT-small with ImageNet [9] pretrained weight as the encoder. At each scale, we use  $Z = 8$  adjacent-view attention layers. Eight NVIDIA 3090 24GB GPUs are used to train our model. Adam [29] is employed as our optimizer with  $\beta_1 = 0.9$  and  $\beta_2 = 0.999$

on both datasets. For the nuScenes [5] datasets, we train the S3Depth with batch size 48, learning rate 1e-4 for 10 epochs. The resolution of input images is downsampled to 640  $\times$  352. When evaluating the models, the resolution of the predicted depth map is upsampled to 900  $\times$  1600. For the DDAD dataset which is larger than nuScenes, we train the S3Depth with batch size 48, learning rate 1e-4 for 20 epochs. The resolution of input images is downsampled to 640  $\times$  384 on DDAD. During the evaluation, the resolution of the predicted depth map is upsampled to 1216  $\times$  1936.

## 4.3. Benchmark Results

**Results on nuScenes.** Because few works study the task of supervised surround-view multi-camera depth estimation, we build a benchmark on the nuScenes [5] dataset. We compare the proposed S3Depth with two methods of self-supervised monocular depth estimation (Monodepth2 [15] and PackNet-SfM [17]), two SOTA self-supervised surround-view depth estimation method (FSM [19] and SurroundDepth [61], as well as two supervised monocular depth estimation (BTS [31] and PixelFormer [1]), as shown

Model	Input	+Adj.	lower is better				higher is better		
			Abs Rel $\downarrow$	Sq Rel $\downarrow$	RMSE $\downarrow$	RMSE log $\downarrow$	$\delta_1 \uparrow$	$\delta_2 \uparrow$	$\delta_3 \uparrow$
ResNet34 [21]	Random		0.091	0.861	3.105	0.178	0.927	0.957	0.972
	Surr.		0.080	0.842	2.882	0.166	0.937	0.961	0.975
	Surr.		0.074	0.755	2.708	0.157	0.945	0.964	0.976
MPViT [32]	Surr.		0.075	0.718	2.703	0.158	0.943	0.964	0.976
	Surr.		<b>0.067</b>	<b>0.673</b>	<b>2.457</b>	<b>0.144</b>	<b>0.951</b>	<b>0.970</b>	<b>0.981</b>

Table 3. The results of depth estimation on nuScenes [5] val set. Adj. stands for Adjacent-view Attention. Random indicates that the input images are selected randomly. Surr. denotes surround-view images captured at the same time

Method	lower is better			
	Abs Rel $\downarrow$	Sq Rel $\downarrow$	RMSE $\downarrow$	RMSE log $\downarrow$
L1 loss	0.067	0.632	2.480	0.145
L1+Smooth loss	0.067	0.673	2.457	0.144
Silog loss	0.069	0.502	2.434	0.135
Silog+Smooth loss	0.068	0.485	2.430	0.134

Table 4. Ablation study of loss on nuScenes [5].

in Table 1. Specifically, we change the supervision of SurroundDepth [61] from self-supervised to LiDAR supervised and get the result from 0.245 to 0.158 in Abs Rel. It is observed that S3Depth respectively reaches 0.067 Abs Rel on the evaluation, which exceeds the recently proposed methods: SurroundDepth (Abs Rel 0.158) and PixelFormer (Abs Rel 0.113). This demonstrates that S3Depth has the ability to further improve the performance of surround-view depth estimation even while SurroundDepth [61] and PixelFormer [1] have achieved impressive performance.

**Results on DDAD.** We also train and test our model in DDAD [17] datasets, which is known for featuring denser depth estimation in challenging conditions when compared to the nuScenes [5] datasets. As indicated in Table 2, our proposed S3Depth also achieves state-of-the-art performance across all evaluation metrics. In addition, we provide qualitative results of different methods on the DDAD [17] dataset in Figure 5. From these results, it is evident that our proposed approach, S3Depth, is capable of predicting more accurate object structures than other competing methods. Our findings suggest that the proposed method can improve the accuracy of depth estimation in challenging conditions and have the potential to be applied in various real-world scenarios.

#### 4.4. Ablation Study

In this subsection, to verify the effects of different modules, we conduct ablation experiments on the nuScenes val set.

**Effect of input.** The first two rows of the Table 3 show the effect of different inputs. It yields better results to use surround-view images as input, compared to using random images. This is because surround-view images have overlapping regions which can stabilize gradients, resulting in improved performance. Specifically, the overlapping regions in surround-view images provide additional information that can improve the accuracy of the model’s predictions.

**Effect of adjacent-view attention.** We conduct the ab-

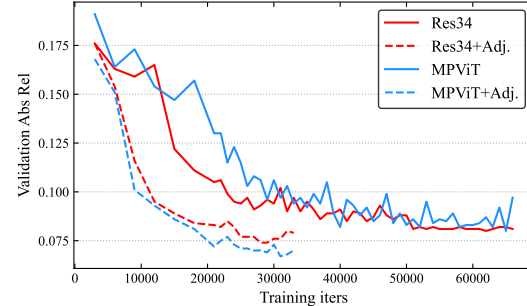


Figure 4. Plot of Abs Rel in the nuScenes [5] val set. Adj. stands for Adjacent-view Attention.

lation study for adjacent-view attention on the nuScenes [5] datasets. As shown in Table 3, the proposed adjacent-attention mechanism facilitates the interaction between adjacent-view information, thereby enabling adjacent-view features to interact with each other. This demonstrates the efficacy of the adjacent-view attention module in enhancing the performance of our model across different backbones. This module effectively enables the network to effectively learn to interact between current and adjacent view features. Moreover, the adjacent-view attention can not only improve the performance but also accelerates the convergence of the model, as shown in Figure 4.

**Effect of loss.** As shown in Table 4, we examine the impact of loss on the performance of our S3Depth. Remarkably, our results indicate that our S3Depth is highly robust to different types of loss functions. This suggests that our model is able to maintain strong performance across a variety of loss functions, demonstrating its versatility and generalizability.

**Effect of backbone.** To delve into the effectiveness of different backbones, we report an ablation study on the nuScenes [5] val set, as shown in Table 5. Also, we report the flops and parameters of different backbones. Benefiting from the module combining CNN and Transformer layers, the MPViT [32] backbone achieves better performance than the pure CNN backbone (ResNet34 [21]). In addition, we further explore the effects of different modules in MPViT [32]. As shown in the bottom of Table 5, both CNN path and Transformer path play an important role in MPViT [32] for depth estimation.

Backbone	Flops	Params	lower is better				higher is better		
			Abs Rel $\downarrow$	Sq Rel $\downarrow$	RMSE $\downarrow$	RMSE log $\downarrow$	$\delta_1 \uparrow$	$\delta_2 \uparrow$	$\delta_3 \uparrow$
ResNet34 [21]	99.19G	27M	0.074	0.755	2.708	0.157	0.945	0.964	0.976
PVT-small [56]	139.14G	7.9M	0.127	1.135	3.842	0.214	0.879	0.927	0.956
MPViT-base [32]	462.33G	78M	<i>OOM</i>	<i>OOM</i>	<i>OOM</i>	<i>OOM</i>	<i>OOM</i>	<i>OOM</i>	<i>OOM</i>
MPViT-tiny [32]	49.53G	<b>10M</b>	0.075	0.787	2.675	0.159	0.944	0.964	0.976
MPViT-xsmall [32]	85.04G	13M	0.069	0.731	2.534	0.150	0.950	0.968	0.979
MPViT-small [32]	134.30G	27M	<b>0.067</b>	<b>0.673</b>	<b>2.457</b>	<b>0.144</b>	<b>0.951</b>	<b>0.970</b>	<b>0.981</b>
MPViT-small [32]	134.30G	27M	<b>0.067</b>	<b>0.673</b>	<b>2.457</b>	<b>0.144</b>	<b>0.951</b>	<b>0.970</b>	<b>0.981</b>
2 Trans. Path	85.04G	10.3M	0.079	0.814	2.726	0.163	0.940	0.962	0.975
1 Trans. Path	82.12G	11.2M	0.076	0.741	2.757	0.163	0.940	0.961	0.974
w/o Trans. Path	57.16G	11.5M	0.082	0.840	2.881	0.170	0.936	0.957	0.971

Table 5. Ablation study of Feature extraction on Nusense [5] val set. Trans. stands for Transformer. Input size is  $640 \times 192$ , and backbone are pre-trained on ImageNet [9]. *OOM* refers to Out Of Memory. All backbones are added Adjacent-view Attention module.

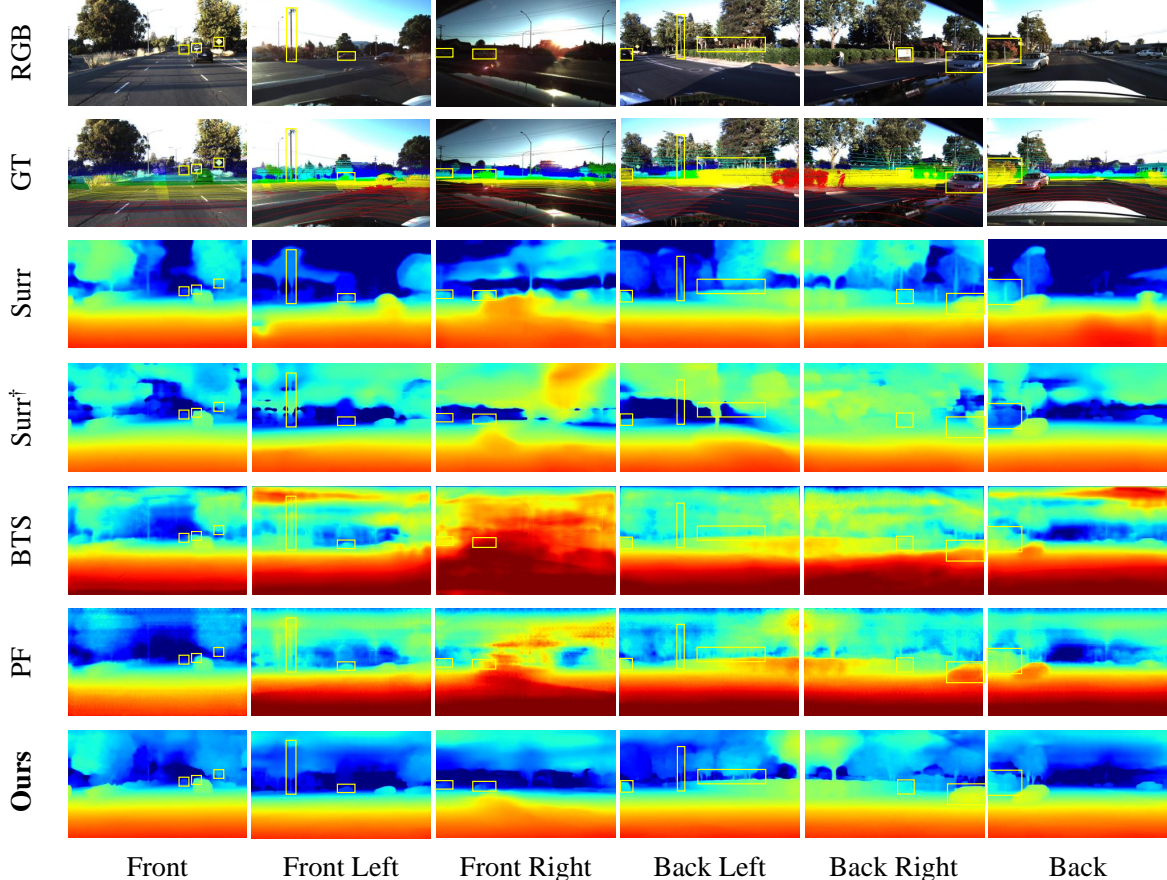


Figure 5. Qualitative results on DDAD [17] dataset. Top two row are input images and GT depth map. Then, the predicted depth maps are provided. Surr indicates SurroundDepth [61], Surr $^{\dagger}$  refers to SurroundDepth [61] supervised with LiDAR. PF denotes PixelFormer [1].

## 5. Conclusion

In this paper, we build a simple baseline for supervised surround-view depth estimation (S3Depth). Different from monocular depth estimation, the core insight of S3Depth is to exchange adjacent-view information and jointly predict all depths of surrounding views. We use a powerful backbone, which combines CNN with transformer layers for enriched representations. Further, adjacent-view attention is employed at multiple and different scales to incorporate adjacent-view features. Through extensive experiments, we

show that S3Depth can achieve state-of-the-art performance on multi-camera depth estimation datasets. We hope the proposed method can serve as a simple and strong baseline for multi-camera depth estimation.

## 6. Limitations

Considering the limitation of our methods, S3Depth depends on the accuracy of the supervised signal. Furthermore, the surround-view and temporal information is needed to be explored.

## References

- [1] Arora C, Agarwal A. Attention attention everywhere: Monocular depth prediction with skip attention. In *WACV*, 2023. [1](#), [2](#), [6](#), [7](#), [8](#)
- [2] Gwangbin Bae, Ignas Budvytis, and Roberto Cipolla. Multi-view depth estimation by fusing single-view depth probability with multi-view geometry. In *CVPR*, 2022. [1](#), [3](#)
- [3] Jia-Wang Bian, Zhichao Li, Naiyan Wang, Huangying Zhan, Chunhua Shen, Ming-Ming Cheng, and Ian Reid. Unsupervised Scale-consistent Depth and Ego-motion Learning from Monocular Video. In *NeurIPS*, 2019. [2](#)
- [4] D. J. Butler, J. Wulff, G. B. Stanley, and M. J. Black. A naturalistic open source movie for optical flow evaluation. In *ECCV*, 2012. [3](#)
- [5] Holger Caesar, Varun Bankiti, Alex H Lang, Sourabh Vora, Venice Erin Liang, Qiang Xu, Anush Krishnan, Yu Pan, Giacomo Baldan, and Oscar Beijbom. muscenes: A multimodal dataset for autonomous driving. In *CVPR*, 2020. [1](#), [2](#), [5](#), [6](#), [7](#), [8](#)
- [6] Nicolas Carion, Francisco Massa, Gabriel Synnaeve, Nicolas Usunier, Alexander Kirillov, and Sergey Zagoruyko. End-to-end object detection with transformers. In *ECCV*, 2020. [4](#)
- [7] Jia-Ren Chang and Yong-Sheng Chen. Pyramid stereo matching network. In *CVPR*, 2018. [1](#), [2](#), [3](#)
- [8] Xuelian Cheng, Yiran Zhong, Mehrtash Harandi, Yuchao Dai, Xiaojun Chang, Hongdong Li, Tom Drummond, and Zongyuan Ge. Hierarchical neural architecture search for deep stereo matching. *NeurIPS*, 2020. [1](#), [3](#)
- [9] Jia Deng, Wei Dong, Richard Socher, Li-Jia Li, Kai Li, and Li Fei-Fei. Imagenet: A large-scale hierarchical image database. In *CVPR*, 2009. [6](#), [8](#)
- [10] Alexey Dosovitskiy, Lucas Beyer, Alexander Kolesnikov, Dirk Weissenborn, Xiaohua Zhai, Thomas Unterthiner, Mostafa Dehghani, Matthias Minderer, Georg Heigold, Sylvain Gelly, et al. An image is worth 16x16 words: Transformers for image recognition at scale. *arXiv preprint arXiv:2010.11929*, 2020. [3](#)
- [11] David Eigen and Rob Fergus. Predicting depth, surface normals and semantic labels with a common multi-scale convolutional architecture. In *ICCV*, 2015. [1](#), [2](#)
- [12] David Eigen, Christian Puhrsch, and Rob Fergus. Depth map prediction from a single image using a multi-scale deep network. *NeurIPS*, 2014. [1](#), [2](#)
- [13] Huan Fu, Mingming Gong, Chaohui Wang, Kayhan Batmanghelich, and Dacheng Tao. Deep ordinal regression network for monocular depth estimation. In *CVPR*, 2018. [1](#), [2](#)
- [14] Andreas Geiger, Philip Lenz, Christoph Stiller, and Raquel Urtasun. Vision meets robotics: The kitti dataset. *INT J ROBOT RES*, 2013. [1](#), [2](#)
- [15] Clément Godard, Oisin Mac Aodha, Michael Firman, and Gabriel J Brostow. Digging into self-supervised monocular depth estimation. In *ICCV*, 2019. [2](#), [3](#), [5](#), [6](#)
- [16] Clément Godard, Oisin Mac Aodha, Michael Firman, and Gabriel J. Brostow. Digging into self-supervised monocular depth prediction. In *ICCV*, 2019. [5](#)
- [17] Vitor Guizilini, Rares Ambrus, Sudeep Pillai, Allan Raventos, and Adrien Gaidon. 3d packing for self-supervised monocular depth estimation. In *CVPR*, 2020. [1](#), [2](#), [3](#), [5](#), [6](#), [7](#), [8](#)
- [18] Vitor Guizilini, Rares Ambrus, Dian Chen, Sergey Zakharov, and Adrien Gaidon. Multi-frame self-supervised depth with transformers. In *CVPR*, 2022. [1](#), [3](#), [4](#)
- [19] Vitor Guizilini, Igor Vasiljevic, Rares Ambrus, Greg Shakhnarovich, and Adrien Gaidon. Full surround monodepth from multiple cameras. *arXiv preprint arXiv:2104.00152*, 2021. [1](#), [3](#), [5](#), [6](#)
- [20] Xiaoyang Guo, Kai Yang, Wukui Yang, Xiaogang Wang, and Hongsheng Li. Group-wise correlation stereo network. In *CVPR*, 2019. [1](#), [3](#)
- [21] Kaiming He, Xiangyu Zhang, Shaoqing Ren, and Jian Sun. Deep residual learning for image recognition. In *CVPR*, 2016. [7](#), [8](#)
- [22] Heiko Hirschmuller. Accurate and efficient stereo processing by semi-global matching and mutual information. In *CVPR*, 2005. [3](#)
- [23] Heiko Hirschmuller. Stereo processing by semiglobal matching and mutual information. *TPAMI*, 2007. [3](#)
- [24] Junjie Hu, Mete Ozay, Yan Zhang, and Takayuki Okatani. Revisiting single image depth estimation: Toward higher resolution maps with accurate object boundaries. In *WACV*, 2019. [1](#), [2](#)
- [25] Gao Huang, Zhuang Liu, Laurens van der Maaten, and Kilian Q Weinberger. Densely connected convolutional networks. In *CVPR*, 2017. [6](#)
- [26] Po-Han Huang, Kevin Matzen, Johannes Kopf, Narendra Ahuja, and Jia-Bin Huang. Deepmvs: Learning multi-view stereopsis. In *CVPR*, 2018. [1](#), [3](#)
- [27] Alex Kendall, Hayk Martirosyan, Saumitro Dasgupta, Peter Henry, Ryan Kennedy, Abraham Bachrach, and Adam Bry. End-to-end learning of geometry and context for deep stereo regression. In *ICCV*, 2017. [1](#), [3](#)
- [28] Sameh Khamis, Sean Fanello, Christoph Rhemann, Adarsh Kowdle, Julien Valentin, and Shahram Izadi. Stereonet: Guided hierarchical refinement for real-time edge-aware depth prediction. In *ECCV*, 2018. [1](#), [3](#)
- [29] Diederik P Kingma and Jimmy Ba. Adam: A method for stochastic optimization. *arXiv preprint arXiv:1412.6980*, 2014. [6](#)
- [30] Iro Laina, Christian Rupprecht, Vasileios Belagiannis, Federico Tombari, and Nassir Navab. Deeper depth prediction with fully convolutional residual networks. In *3DV*, 2016. [1](#), [2](#)
- [31] Jin Han Lee, Myung-Kyu Han, Dong Wook Ko, and Il Hong Suh. From big to small: Multi-scale local planar guidance for monocular depth estimation. *arXiv preprint arXiv:1907.10326*, 2019. [6](#)
- [32] Youngwan Lee, Jonghee Kim, Jeff Willette, and Sung Ju Hwang. Mpvit: Multi-path vision transformer for dense prediction. *arXiv preprint arXiv:2112.11010*, 2021. [3](#), [4](#), [7](#), [8](#)
- [33] Yinhao Li, Han Bao, Zheng Ge, Jinrong Yang, Jianjian Sun, and Zeming Li. Bevstereo: Enhancing depth estimation in multi-view 3d object detection with dynamic temporal stereo. In *arXiv preprint arXiv:2209.10248v1*, 2022. [2](#), [3](#)

- [34] Yinhao Li, Zheng Ge, Guanyi Yu, Jinrong Yang, Zengran Wang, Yukang Shi, Jianjian Sun, and Zeming Li. Bevdepth: Acquisition of reliable depth for multi-view 3d object detection. *arXiv preprint arXiv:2206.10092*, 2022. [1](#), [2](#), [3](#)
- [35] Zhaoshuo Li, Xingtong Liu, Nathan Drenkow, Andy Ding, Francis X. Creighton, Russell H. Taylor, and Mathias Uebelath. Revisiting stereo depth estimation from a sequence-to-sequence perspective with transformers. In *ICCV*, 2021. [1](#), [3](#)
- [36] Zhenyu Li, Xuyang Wang, Xianming Liu, and Junjun Jiang. Binsformer: Revisiting adaptive bins for monocular depth estimation. *arXiv preprint arXiv:2204.00987*, 2022. [2](#)
- [37] Zhengfa Liang, Yiliu Feng, Yulan Guo, Hengzhu Liu, Wei Chen, Linbo Qiao, Li Zhou, and Jianfeng Zhang. Learning for disparity estimation through feature constancy. In *CVPR*, 2018. [1](#), [3](#)
- [38] Ce Liu, Suryansh Kumar, Shuhang Gu, Radu Timofte, and Luc Van Gool. Va-depthnet: A variational approach to single image depth prediction. *arXiv preprint arXiv:2302.06556*, 2023. [2](#)
- [39] Faya Liu, Chunhua Shen, and Guosheng Lin. Deep convolutional neural fields for depth estimation from a single image. In *CVPR*, 2015. [1](#), [2](#)
- [40] Miaomiao Liu, Mathieu Salzmann, and Xuming He. Discrete-continuous depth estimation from a single image. In *CVPR*, 2014. [2](#)
- [41] Ze Liu, Yutong Lin, Yue Cao, Han Hu, Yixuan Wei, Zheng Zhang, Stephen Lin, and Baining Guo. Swin transformer: Hierarchical vision transformer using shifted windows. In *ICCV*, 2021. [3](#), [4](#), [6](#)
- [42] Nikolaus Mayer, Eddy Ilg, Philip Hausser, Philipp Fischer, Daniel Cremers, Alexey Dosovitskiy, and Thomas Brox. A large dataset to train convolutional networks for disparity, optical flow, and scene flow estimation. In *CVPR*, 2016. [1](#), [3](#)
- [43] Pushmeet Kohli, Nathan Silberman, Derek Hoiem and Rob Fergus. Indoor segmentation and support inference from rgbd images. In *ECCV*, 2012. [2](#)
- [44] Jiahao Pang, Wenxiu Sun, Jimmy SJ Ren, Chengxi Yang, and Qiong Yan. Cascade residual learning: A two-stage convolutional neural network for stereo matching. In *CVPRW*, 2017. [1](#), [3](#)
- [45] Adam Paszke, Sam Gross, Francisco Massa, Adam Lerer, James Bradbury, Gregory Chanan, Trevor Killeen, Zeming Lin, Natalia Gimelshein, Luca Antiga, Alban Desmaison, Andreas Kopf, Edward Yang, Zachary DeVito, Martin Raison, Alykhan Tejani, Sasank Chilamkurthy, Benoit Steiner, Lu Fang, Junjie Bai, and Soumith Chintala. Pytorch: An imperative style, high-performance deep learning library. In H. Wallach, H. Larochelle, A. Beygelzimer, F. d'Alché-Buc, E. Fox, and R. Garnett, editors, *NeurIPS*. 2019. [6](#)
- [46] Vaishakh Patil, Christos Sakaridis, Alex Liniger, and Luc Van Gool. P3depth: Monocular depth estimation with a piecewise planarity prior. In *CVPR*, 2022. [2](#)
- [47] René Ranftl, Alexey Bochkovskiy, and Vladlen Koltun. Vision transformers for dense prediction. In *ICCV*, 2021. [3](#), [4](#)
- [48] Anurag Ranjan, Varun Jampani, Lukas Balles, Kihwan Kim, Deqing Sun, Jonas Wulff, and Michael J Black. Competitive collaboration: Joint unsupervised learning of depth, camera motion, optical flow and motion segmentation. In *CVPR*, 2019. [2](#)
- [49] Ashutosh Saxena, Min Sun, and Andrew Y Ng. Make3d: Learning 3d scene structure from a single still image. *TPAMI*, 2008. [1](#), [2](#)
- [50] Ashutosh Saxena, Min Sun, and Andrew Y Ng. Make3d: Learning 3d scene structure from a single still image. In *TPAMI*, 2009. [2](#)
- [51] Johannes L Schonberger and Jan-Michael Frahm. Structure-from-motion revisited. In *CVPR*, 2016. [3](#)
- [52] Shuwei Shao, Zhongcai Pei, Weihai Chen, Ran Li, Zhong Liu, and Zhengguo Li. Urcdc-depth: Uncertainty rectified cross-distillation with cutflip for monocular depth estimation. *arXiv preprint arXiv:2302.08149*, 2023. [2](#)
- [53] Vladimir Tankovich, Christian Hane, Yinda Zhang, Adarsh Kowdle, Sean Fanello, and Sofien Bouaziz. Hitnet: Hierarchical iterative tile refinement network for real-time stereo matching. In *CVPR*, 2021. [1](#), [3](#)
- [54] Jonathan Tremblay, Thang To, and Stan Birchfield. Falling things: A synthetic dataset for 3d object detection and pose estimation. In *CVPRW*, 2018. [3](#)
- [55] Qiang Wang, Shaohuai Shi, Shizhen Zheng, Kaiyong Zhao, and Xiaowen Chu. FADNet: A fast and accurate network for disparity estimation. In *ICRA*, 2020. [1](#), [3](#)
- [56] Wenhui Wang, Enze Xie, Xiang Li, Deng-Ping Fan, Kaitao Song, Ding Liang, Tong Lu, Ping Luo, and Ling Shao. Pyramid vision transformer: A versatile backbone for dense prediction without convolutions. In *ICCV*, 2021. [8](#)
- [57] Zengran Wang, Chen Min, Zheng Ge, Yinhao Li, Zeming Li, Hongyu Yang, and Di Huang. Sts: Surround-view temporal stereo for multi-view 3d detection. *arXiv preprint arXiv:2208.10145*, 2022. [1](#), [3](#)
- [58] Zhongdao Wang, Luming Tang, Xihui Liu, Zhuliang Yao, Shuai Yi, Jing Shao, Junjie Yan, Shengjin Wang, Hongsheng Li, and Xiaogang Wang. Orientation invariant feature embedding and spatial temporal regularization for vehicle re-identification. In *ICCV*, 2017. [2](#)
- [59] Jamie Watson, Oisin Mac Aodha, Victor Prisacariu, Gabriel Brostow, and Michael Firman. The temporal opportunist: Self-supervised multi-frame monocular depth. In *CVPR*, 2021. [1](#), [3](#)
- [60] Yi Wei, Shaohui Liu, Yongming Rao, Wang Zhao, Jiwen Lu, and Jie Zhou. Nerfingmvs: Guided optimization of neural radiance fields for indoor multi-view stereo. In *ICCV*, 2021. [1](#), [3](#)
- [61] Yi Wei, Linqing Zhao, Wenzhao Zheng, Zheng Zhu, Yongming Rao, Guan Huang, Jiwen Lu, and Jie Zhou. Surrounddepth: Entangling surrounding views for self-supervised multi-camera depth estimation. *arXiv preprint arXiv:2204.03636*, 2022. [1](#), [3](#), [4](#), [5](#), [6](#), [7](#), [8](#)
- [62] Felix Wimbauer, Nan Yang, Lukas Von Stumberg, Niclas Zeller, and Daniel Cremers. Monorec: Semi-supervised dense reconstruction in dynamic environments from a single moving camera. In *CVPR*, 2021. [1](#), [3](#)
- [63] Dan Xu, Wei Wang, Hao Tang, Hong Liu, Nicu Sebe, and Elisa Ricci. Structured attention guided convolutional neural fields for monocular depth estimation. In *CVPR*, 2018. [1](#), [2](#)

- [64] Haofei Xu and Juyong Zhang. Aanet: Adaptive aggregation network for efficient stereo matching. In *CVPR*, 2020. [1](#), [3](#)
- [65] Youze Xue, Jiansheng Chen, Weitao Wan, Yiqing Huang, Cheng Yu, Tianpeng Li, and Jiayu Bao. Mvscrf: Learning multi-view stereo with conditional random fields. In *ICCV*, 2019. [1](#), [3](#)
- [66] Gengshan Yang, Joshua Manela, Michael Happold, and Deva Ramanan. Hierarchical deep stereo matching on high-resolution images. In *CVPR*, 2019. [1](#), [3](#)
- [67] Guanglei Yang, Hao Tang, Mingli Ding, Nicu Sebe, and Elisa Ricci. Transformer-based attention networks for continuous pixel-wise prediction. In *ICCV*, 2021. [3](#), [4](#)
- [68] Yao Yao, Zixin Luo, Shiwei Li, Tian Fang, and Long Quan. Mvsnet: Depth inference for unstructured multi-view stereo. In *ECCV*, 2018. [1](#), [3](#)
- [69] Wei Yin, Yifan Liu, Chunhua Shen, and Youliang Yan. Enforcing geometric constraints of virtual normal for depth prediction. In *ICCV*, 2019. [1](#), [2](#)
- [70] Zhichao Yin and Jianping Shi. Geonet: Unsupervised learning of dense depth, optical flow and camera pose. In *CVPR*, 2018. [2](#)
- [71] Weihao Yuan, Xiaodong Gu, Zuozhuo Dai, Siyu Zhu, and Ping Tan. Neural window fully-connected crfs for monocular depth estimation. In *CVPR*, 2022. [2](#)
- [72] Feihu Zhang, Victor Prisacariu, Ruigang Yang, and Philip HS Torr. Ga-net: Guided aggregation net for end-to-end stereo matching. In *CVPR*, 2019. [1](#), [3](#)
- [73] Chaoqiang Zhao, Youmin Zhang, Matteo Poggi, Fabio Tosi, Xianda Guo, Zheng Zhu, Guan Huang, Yang Tang, and Stefano Mattoccia. Monovit: Self-supervised monocular depth estimation with a vision transformer. In *3DV*, 2022. [1](#), [3](#), [4](#)
- [74] Wang Zhao, Shaohui Liu, Yezhi Shu, and Yong-Jin Liu. Towards Better Generalization: Joint Depth-Pose Learning without PoseNet. In *CVPR*, 2020. [2](#)
- [75] Junsheng Zhou, Yuwang Wang, Kaihuai Qin, and Wenjun Zeng. Moving Indoor: Unsupervised Video Depth Learning in Challenging Environments. In *ICCV*, 2019. [2](#)
- [76] Tinghui Zhou, Matthew Brown, Noah Snavely, and David G Lowe. Unsupervised learning of depth and ego-motion from video. In *CVPR*, 2017. [2](#), [3](#)
- [77] Wei Zhuo, Mathieu Salzmann, Xuming He, and Miaomiao Liu. Indoor scene structure analysis for single image depth estimation. In *CVPR*, 2015. [2](#)